JACS
JOURNAL OF THE AMERICAN CHEMICAL SOCIETY
Article
pubs.acs.org/JACS

Tunneling Interlayer for Efficient Transport of Charges in Metal Oxide Electrodes

Jiazang Chen,[†,‡] Liping Zhang,[†] Zhenhui Lam,[†] Hua Bing Tao,[†] Zhiping Zeng,[†] Hong Bin Yang,[†] Jianqiang Luo,[†] Lin Ma,[†] Bo Li,[§] Jianfeng Zheng,[‡] Suping Jia,[‡] Zhijian Wang,[‡] Zhenping Zhu,*[,‡] and Bin Liu*[,†]

[†]School of Chemical & Biomedical Engineering, Nanyang Technological University, 62 Nanyang Drive, Singapore 637459, Singapore
[‡]State Key Laboratory of Coal Conversion, Institute of Coal Chemistry, Chinese Academy of Sciences, Taiyuan 030001, China
[§]Lanzhou Petrochemical Research Center of Petrochemical Research Institute, PetroChina, Lanzhou 730060, China

Supporting Information

ABSTRACT: Due to the limited electronic conductivity, the application of many metal oxides that may have attractive (photo)-electrochemical properties has been limited. Regarding these issues, incorporating low-dimensional conducting scaffolds into the electrodes or supporting the metal oxides onto the conducting networks are common approaches. However, some key electronic processes like interfacial charge transfer are far from being consciously concerned. Here we use a carbon-TiO_2 contact as a model system to demonstrate the electronic processes occurring at the metal−semiconductor interface. To minimize the energy dissipation for fast transfer of electrons from semiconductor to carbon scaffolds, facilitating electron tunneling while avoiding high energy-consuming thermionic emission is desired, according to our theoretical simulation of the voltammetric behaviors. To validate this, we manage to sandwich ultrathin TiO_2 interlayers with heavy electronic doping between the carbon conductors and dopant-free TiO_2. The radially graded distribution of the electronic doping along the cross-sectional direction of carbon conductor realized by immobilizing the dopant species on the carbon surface can minimize the energy consumption for contacts to both the carbon and the dopant-free TiO_2. Our strategy provides an important requirement for metal oxide electrode design.

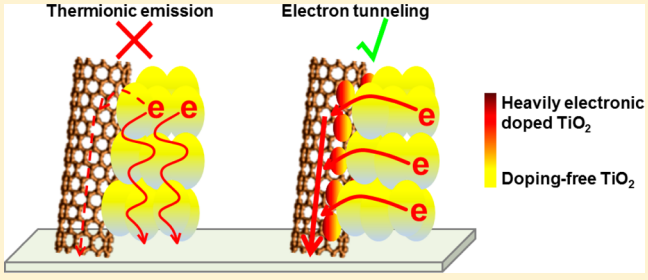

1. INTRODUCTION

Due to the limited electronic conductivity, the intrinsic electrochemical characteristics of many metal oxides that may have promising electrocatalytic activity for interfacial reactions are severely restricted.[1−5] The same phenomenon is also common in photoelectrochemical (PEC) cells, in which the collection of charges is less efficient than the ability to generate upon photoinduced processes, because of the limited charge transport in the semiconductor electrodes.[6] Thus far, many approaches, including formation of aligned arrays,[7,8] modulation of the intraband electronic states of the semiconductor,[9−14] and the most exemplificative strategy, adoption of heterogeneous three-dimensional conducting networks (carbon nanostructures such as carbon nanotubes and graphene sheets are the most common) as special charge-transport channels to incorporate into the semiconductor electrodes and/or to support the metal oxide nanostructures, have been proposed.[3,4,15−26] Despite intensive efforts, facilitating the transport of charges in the semiconductor electrodes is still far from being satisfactory. Transport of charges in the semiconductor electrodes based on these elaborately designed electrodes is only marginally faster than that in nanoparticulate films,[27−29] due to the larger internal energy dissipation arising from the homogeneous/heterogeneous boundary charge transfer compared with that in the case of pure nanoparticles.[27−30] Although charge transfer within the semiconductor electrodes plays a predominant role in limiting transport, the relationship between the electrode configuration and transport of charges, which has been expected to guide the designing of efficient (photo)-electrochemical devices, is undesirably obscured.[31]

Transport of charges in semiconductor electrodes is the most concerned issue. However, the designing of electrode configuration is to some extent intuitive, as the information on the electronic processes occurring in the semiconductor electrodes is usually hidden from the tangible investigations (e.g., electron microscopy).[31,32] It is believed that in carbon nanostructures incorporated TiO_2 electrodes, the electrons can directly transfer to the conducting substrate via the carbon conductors, without encountering the numerous grain boundaries during the transport of electrons through the mesoporous films.[23,25,33−37] However, the behaviors of the charge transfer through the heterogeneous interface from TiO_2 to the carbon network have hardly been investigated,[30] and the

Received: December 24, 2015
Published: February 11, 2016

DOI: 10.1021/jacs.5b13464
J. Am. Chem. Soc. 2016, 138, 3183−3189

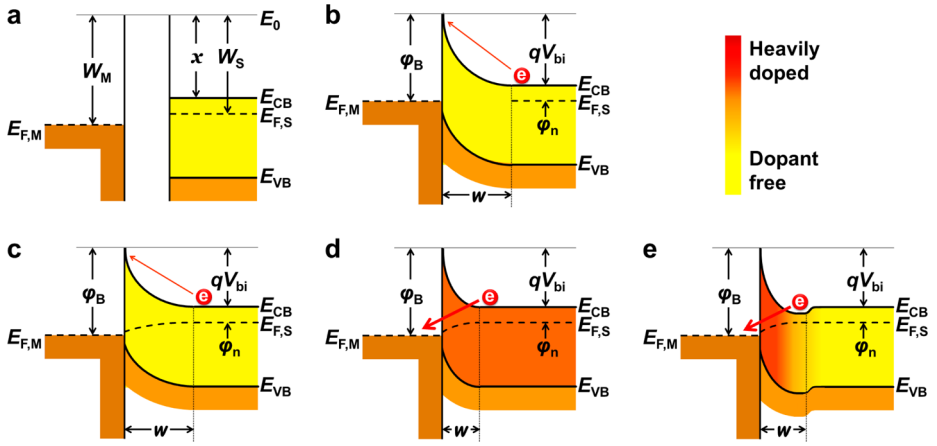

Figure 1. Energy band diagrams for isolated metal and semiconductor (a) and the formed metal−semiconductor contact (b−e). It can be seen that the band in the semiconductor side of the formed contact is bent upward (b−e). The potential barrier height (φ_B) of the metal−semiconductor contact can be given by $\varphi_B = W_m - \chi$, where W_m is work function of the metal, and χ is the electron affinity of the semiconductor. On the semiconductor side, the built-in potential barrier (qV_{bi}) can be obtained by $qV_{bi} = \varphi_B - \varphi_n - qV_D$, where V_D is the bias potential applied to the contact. In the case of doping-free semiconductor, the barrier for transfer of electrons from semiconductor to the metal by thermionic emission becomes smaller as the forward bias increases (b, c). By electronic doping of the semiconductor, the width of the space charge layer becomes narrower and electron tunneling emerges to be the predominant charge-transfer behaviors (d). Efficient electron tunneling can also be realized by selectively doping the semiconductor, in which the semiconductor is only electronically doped near the S−M interface, while the bulk remains dopant-free (e).

potential-dependent energy consumption for the charges across the barriers following thermionic emission in some PEC and electrochemical cells is too large to be tolerable.[30,38−40]

Electron tunneling offers a potential solution by reducing the internal energy dissipation for charge transfer through the semiconductor−metal (S−M) interface.[41−44] Here, we present an analysis to estimate the charge-transfer-dependent energy dissipation and propose a strategy to facilitate charge transfer by electron tunneling. To generalize our strategy, we adopt carbon nanotube (CNT) incorporated TiO_2-based PEC devices to demonstrate the energy saving by electron tunneling, because the carbon-TiO_2 contact is very common in many applications not limited to composite electrodes, but also for the carbon (graphite or glassy carbon) supported electrocatalysts/photocatalysts. Furthermore, this type of cell possesses substantially high current densities (e.g., 5−20 mA/cm^2), making them representative for the most of the (photo)-electrochemical systems.

2. RESULTS AND DISCUSSION

2.1. Development of Electron Tunneling Model for CNTs-TiO_2 Interfacial Charge Transfer. Transfer of electrons from TiO_2 into the carbon nanostructures is not only the prerequisite to play the role of charge transport channels in semiconductor electrodes but also a basic requirement for the efficient charge separation for carbon composited TiO_2 electrodes/(photo)-catalysts. According to contact theory, transfer of electrons through the S−M interface can be realized by two major approaches: thermionic emission and electron tunneling.[41] Under forward bias, the manner of charge transfer on the S−M interface mainly depends on the height (φ_B) and the width (w) of the potential barriers (Figure 1). To remain the intrinsic properties and/or reduce the charge loss by interfacial recombination, the TiO_2 used for fabrication of (photo)-electrochemical cells (e.g., dye-/quantum dot-sensitized solar cells, DSSCs/QDSSCs) is almost dopant-free. Thus, it would be appropriate to apply thermionic emission to describe the transfer of charges from the semiconductor to the metals (e.g., carbon).[30,39] However, charge transfer by thermionic emission will consume a large amount of energy if the Schottky barrier height is larger than 0.5 eV (Figure S1), which will result undesirably in a lowering of energy output.[38−40] For the case of carbon and TiO_2, the height of Schottky barrier reaches as high as 0.75 eV (by adopting 4.95 eV as the work function for carbon nanotubes and −4.2 eV for the conduction band level for TiO_2).[45] Thus, it is not surprising that the photocurrent−voltage (J−V) characteristics of the devices based on carbon nanostructures composited TiO_2 electrodes offset the normal photovoltaic behaviors of semiconductor−liquid junction cells.[18,20−22,25,37,46−50]

Reducing the width of the potential barriers to increase the probability of electron tunneling seems to be a rational approach to facilitate the charge transfer through the S−M interface and to reduce the internal energy dissipation (Figures S2−S4). Generally, reducing the width of the potential barriers can be simply realized by increasing the density of electronic doping in the semiconductor (Figures 1d and S4).[51] However, increasing the density of electronic doping will simultaneously increase the probability of trapping/detrapping events during the operation of the cells and aggravate the charge loss at semiconductor−electrolyte interface (SEI).[52]

To fully exert the function of the carbon conductor to facilitate the charge collection while avoiding severe charge recombination at SEI, it is rational to selectively dope the semiconductor to electrically bridge the S−M interface (Figure 1e). In this work, inspired by the simulated J−V behaviors (Figure 2a) with consideration of electron tunneling, we adopt heavily electronically doped ultrathin TiO_2 layers as the intermediate to connect the doping-free TiO_2 nanoparticles and the CNTs (Figures 1e and 2b). To demonstrate the intrinsic superiority of the intermediate bridging, electronic process manner and PEC behaviors occurring in the CNT-TiO_2 electrodes were investigated.

Figure 2b shows the schematic diagram of the electrode configuration as we proposed. The intermediate ultrathin electronically doped TiO_2 layers are sandwiched between the

DOI: 10.1021/jacs.5b13464
J. Am. Chem. Soc. 2016, 138, 3183−3189

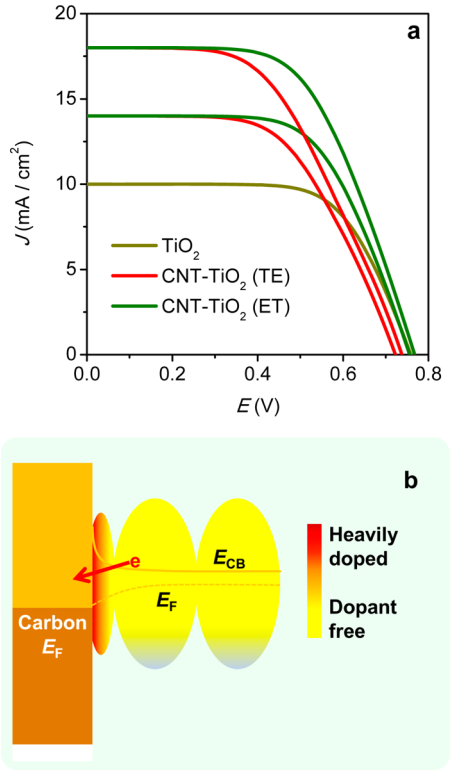

Figure 2. Features of the composite electrodes with efficient electron tunneling through the TiO_2−carbon interface. (a) Effect of interfacial charge-transfer behaviors on the J−V features of the photovoltaic cells based on CNTs incorporated TiO_2 electrodes. The simulated J−V curves show that the charge transfer through the CNT−TiO_2 interface by electron tunneling (ET) can effectively reduce the internal energy dissipation, as compared with the case of thermionic emission (TE). The parameters adopted for the simulation are ideality factor, m = 1.8; saturation current, $J_0 = 1 \times 10^{-5}$ mA/cm^2; series resistance, R_s = 10 Ω; height of carbon-TiO_2 barrier, φ_B = 0.75 eV; height of FTO-TiO_2 barrier, φ_B = 0.2 eV; the density of electronic doping of TiO_2 for the case of electron tunneling is 1×10^{21} cm^{-3}; the short-circuit photocurrent densities, J_{SC} = 10.00 mA/cm^2 for the plain cells and increased to 14 and 18 mA/cm^2 for the cells with CNTs incorporated TiO_2 electrodes to show the benefit of charge collection improvement. (b) Schematic illustration of hierarchical allocations of electronic doping in the CNTs incorporated TiO_2 electrodes. The small-sized TiO_2 contact to the CNTs is heavily electronically doped by foreign elements like niobium.

carbon conductors and the doping-free TiO_2 building blocks in the electrodes. One important feature for the intermediate layers is the density of electronic doping, which is a graded distribution along the radial direction of the CNTs. To facilitate the charge transfer by electron tunneling, the density of electronic doping near the S−M interface is kept high, while it becomes lower as it walks away from the CNTs. On the boundary to the doping-free TiO_2, the intergrain difference in electronic structures disappears. In this situation, the electrons in the TiO_2 nanostructures, which are photogenerated by light excitation or injected from other excited light absorbers, can be collected by the tubular carbon nanostructures by passing through the heavily electronically doped TiO_2 ultrathin layers, without severely consuming the energy. Besides, in this type of electrode configuration, the introduction of electronic doping will not aggravate the charge loss by interfacial recombination, owing to the fact that the highly doped TiO_2 is concentrated in the vicinity of the interface to CNTs and has no chance to access the electron acceptors in the electrolyte.

2.2. Growth of Ultrathin TiO_2 Layer with Graded Distribution of Niobium Dopants on Carbon Nanotubes. To validate the theoretical prediction, it is required to prepare electronically doped TiO_2 ultrathin layer coated CNTs. Niobium is a common foreign element to realize electronic doping for TiO_2 with a wide range of dopant concentrations.[53] To achieve graded distribution of the niobium dopants along the radial direction of CNTs, we first immobilize the guest metal molecules (ions) on the surface of the carbon nanostructures by chelating the surface functional groups like carboxylic groups with their empty d-orbitals (Figure S5).[54] After that, ethylenediamine is employed to connect the dopant precursor with the host titanium-containing molecules through its electrophilic group in the tips of the molecules (Figures S5 and S6). Finally, the ultrathin TiO_2 layer with radially graded distribution of niobium dopants (denoted CNT|Nb-TiO_2(t)) can be grown on CNTs by dehydrating the precursor-coated CNTs (Figures 3 and S5−S7). To demonstrate the effect of electronic doping, TiO_2 ultrathin layer coated CNTs without niobium dopant (denoted CNT|TiO_2(t)) was also prepared by a similar method without introducing niobium precursor (Figure S8).

Figure 3a−c present the scanning electron microscopy (SEM) images of the CNTs before and after modification of ultrathin (niobium-doped) TiO_2 layers. The increase in the diameter and the surface roughness suggest the successful coating of TiO_2 layers on the CNTs. By introduction of niobium precursor into the reaction system, it can be seen that the dopant is of graded distribution along the radial direction of CNTs (Figure S9) and does not alter the thickness of TiO_2 coating layers (Figure S7). X-ray diffraction (XRD) patterns show that both TiO_2 ultrathin coatings with and without niobium doping are of the anatase phase (Figure 3d). The absence of niobium oxide and other niobium-containing species in the XRD pattern suggests that all niobium are doped into the TiO_2 layers. The significant broadening of the (101) diffraction peak for the CNT|Nb-TiO_2(t) sample indicates distortion of the TiO_2 lattice, resulting most likely from the doping by niobium (inset of Figure 3d).[53] Raman spectroscopy provides a detailed structural probe of local coordination environments.[55] The broadening of all Raman peaks and the blue shift of the characteristic $E_{g(1)}$ mode as well as the red shift of $E_{g(3)}$ mode suggests that the electronic structures have been modified by introduction of niobium into the TiO_2 (Figure 3e). Besides, the appearance of the Nb 3d signal and broadening of Ti 2p peaks in the X-ray photoelectron spectroscopy (XPS) spectra further confirm the successful niobium doping in the CNT|Nb-TiO_2(t) sample (Figure S10).

2.3. Energy Saving by Electron Tunneling. As studied previously,[19,33] the introduction of conducting scaffold into mesoporous TiO_2 electrodes can improve the charge collection by reducing the boundary scattering of electrons during the charge transport processes. The increase in the short-circuit photocurrent density as shown in the photovoltaic characteristics reveals that the introduction of CNTs into mesoporous TiO_2 electrodes can indeed improve the electron transport (Figure 4). However, due to different charge-transfer behaviors across the S−M interface, the increment of photocurrent for individual cell is rather different. The reference cell without CNTs exhibits the lowest photocurrent density (J_{SC}, 10.18 mA/cm^2) and energy conversion efficiency (η, 5.31%, Figure 4a).

DOI: 10.1021/jacs.5b13464
J. Am. Chem. Soc. 2016, 138, 3183−3189

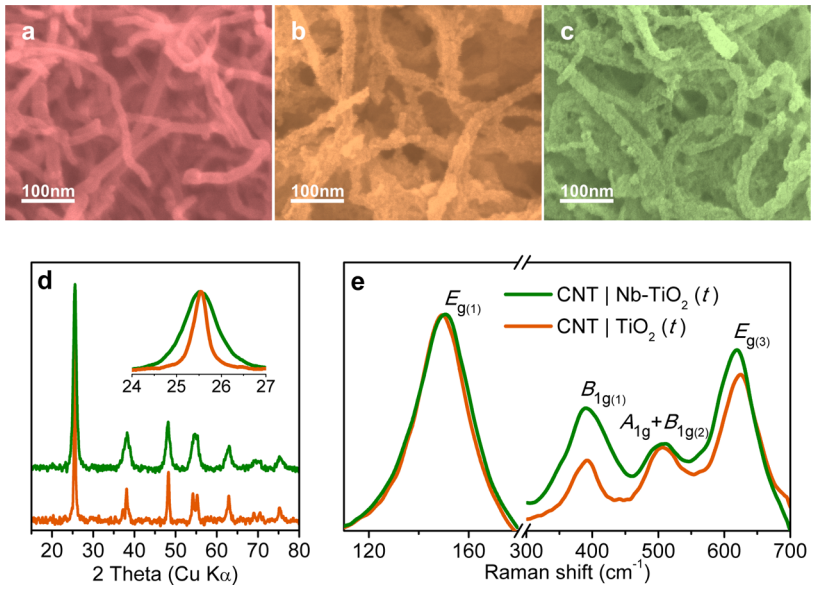

Figure 3. Features of the ultrathin TiO_2 coating layers on the CNTs. SEM images for the CNT-COOH before (a) and after coating with ultrathin TiO_2 (b) and niobium-doped TiO_2 (c) layers. XRD patterns (d) and Raman spectra (e) for CNT|TiO_2(t) and CNT|Nb-TiO_2(t) samples.

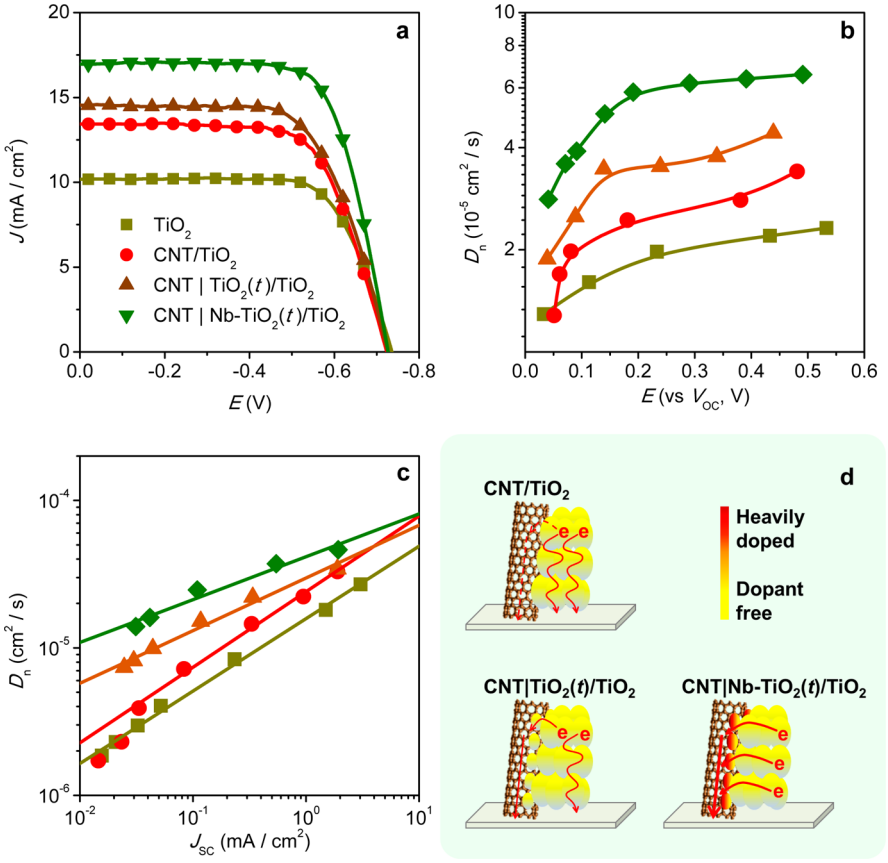

Figure 4. Photovoltaic characteristics of the cells based on CNTs-TiO_2 electrodes. (a) Photocurrent−voltage characteristics of the cells with various CNT-TiO_2 electrodes. (b) Diffusion coefficients of photogenerated electrons in the semiconductor electrodes of the cells under bias versus the open-circuit potentials. (c) Diffusion coefficients of the photogenerated electrons in semiconductor electrodes under various illumination intensities. (d) Schematic diagrams for the electronic processes occurring in CNTs incorporated TiO_2 electrodes with various situations of CNT-TiO_2 contact. The dashed arrow shown in the CNT/TiO_2 electrode (upper left) indicates that the transfer of charges from TiO_2 to CNTs by thermionic emission is not always available. By placing the ultrathin TiO_2 layers between the CNTs and dopant-free TiO_2, charge transfer through the CNT-TiO_2 interface becomes considerable as electron tunneling emerges (thin arrow in the bottom left panel). In the CNT|Nb-TiO_2(t) incorporated TiO_2 electrode, CNTs fully exert the role of charge transport channels, as the electron tunneling for the charge transfer through the CNTs-TiO_2 interface is very obvious.

DOI: 10.1021/jacs.5b13464
J. Am. Chem. Soc. 2016, 138, 3183−3189

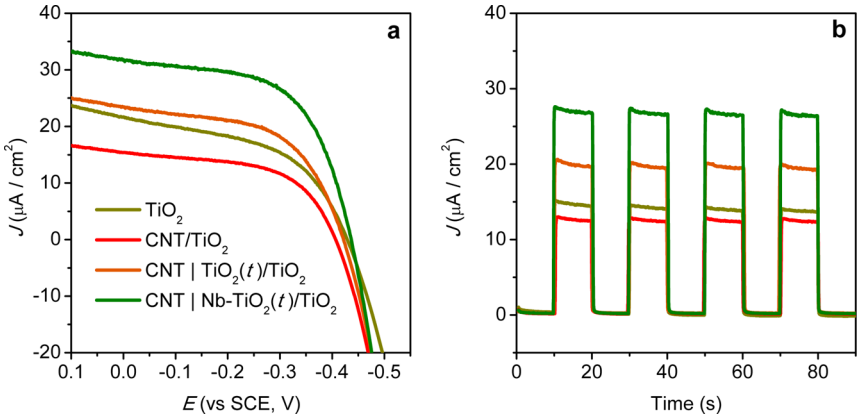

Figure 5. Voltammetric behaviors (a) and photocurrent responses (b) of the PEC cells under AM 1.5G illumination.

Following an ascending order in performance is the cell using CNT incorporated TiO_2 (CNT/TiO_2) electrodes, which exhibits 13.43 mA/cm^2 and 6.55% for J_{SC} and η, respectively. The cell with $CNT|TiO_2(t)$ incorporated TiO_2 electrodes exhibits a continuously increased photocurrent density (J_{SC} = 14.55 mA/cm^2) and energy conversion efficiency (η = 6.94%), due likely to the suppression of interfacial charge leakage via the carbon nanostructures.[30] The cells with $CNT|Nb\text{-}TiO_2(t)$ incorporated TiO_2 electrodes exhibit the best performance, showing 8.69% of energy conversion efficiency and 16.92 mA/cm^2 of short-circuit photocurrent density. Among the photovoltaic parameters, it is clear that J_{SC} is very sensitive to the electron transport processes, which plays the predominant role on the variation of η for all of the cells.

The improvement in charge collection for the CNTs-containing TiO_2 electrodes is strongly dependent on the transfer behaviors of the photogenerated electrons from the semiconductor to the carbon conducting scaffolds. This is to say that the energy dissipation for the transfer of charge through the S−M interface eventually determines the role of the charge-transport channels. For the CNT/TiO_2 electrode, the situation is very similar to the Schottky contact of doping-free semiconductor to metal, in which thermionic emission is the predominant manner for transfer of charges. As the potential barriers for CNT-TiO_2 contact reaches as high as 0.75 eV, the energy consumption for the charge transfer across the TiO_2−CNT interface is very high (Figure S1). As a result, only a certain percentage of electrons can overcome the barrier and transfer into the carbon conductor. The situation becomes even worse in the region where the band bending is large (Figure 4b,c).[30] Therefore, the function of charge-transport channels will be restricted, and improvement in the charge collection will be limited in CNT/TiO_2 electrode (Figure 4a,d).

Introducing electronically doped TiO_2 ultrathin layers into the CNTs incorporated electrodes ($CNT|Nb\text{-}TiO_2(t)/TiO_2$) greatly improves the charge collection and charge diffusion coefficient (D_n). It is well-known that the probability of electron tunneling from semiconductor to metal increases with an increase in density of electronic doping in the semiconductor phase (Figure S4), which in-turn lowers the energy consumption for charge transfer (Figure S2). Here in our case, the average electronic doping density of the TiO_2 in the $CNT|Nb\text{-}TiO_2(t)$ sample reaches as high as 1.79×10^{21} cm^{-3} (Figure S11), which is much higher than that of common doping-free TiO_2 nanoparticles (7.15×10^{18} cm^{-3}). Thus, in our $CNT|Nb\text{-}TiO_2(t)/TiO_2$ electrodes, the carbon networks could fully exert the function of charge-transport channels by reducing the energy dissipation for charge transfer across the TiO_2−CNT interfaces via electron tunneling through highly electronically doped intermediate layers. Therefore, electrons will take the energetically favorable pathways to reach the substrate by eliminating the multiple TiO_2 particle−particle boundary scatterings. Since the energy dissipation for charge transfer through the S−M interface is very low, the improvement in charge transport is still evident even in the case of low photocurrent densities, in which the band bending is very high and the thermionic emission is almost forbidden (Figure 4b−d).

It is noteworthy that the introduction of $CNT|TiO_2(t)$ into the TiO_2 electrodes not only improves the charge collection and J_{SC} but also increases the charge diffusion coefficient (Figure 4b,c), as compared with the case of CNT/TiO_2 electrode, especially in the region of low photocurrent densities, in which the thermionic emission is insignificant. It is expected that coating CNTs with ultrathin TiO_2 layers can improve the charge collection by effectively suppressing interfacial charge leakage via the naked part of carbon.[56] The increase in charge diffusion coefficient should be ascribed to electron tunneling due to the following reason: Generally, in nanostructured semiconductor electrodes, the major potential drop can be confined in the first few layers of the nanoparticles in contact to the metal-like conductor (Figure S12).[57] In our case, the thickness of the ultrathin TiO_2 coating in $CNT|TiO_2(t)$ is only ∼4 nm (Figure S7), which is similar to the critical thickness to tunnel a considerable current.[42−44] As a result, transfer of charges through the S−M interface by means of electron tunneling should occur favorably, which is helpful to facilitate charge transport as well as increase the charge diffusion coefficient (Figure 4b−d).

To further verify the validity of the merits of electron tunneling to charge collection at low current conditions, we examined the photoinduced voltammetric behaviors of naked TiO_2 electrodes in a trielectrode water splitting system (Figure 5). As the porous electrode is unsensitized, it can only generate a small photocurrent by absorbing the ultraviolet photons in the solar spectrum. The PEC results once again confirm that the heavily electronically doped TiO_2 ultrathin layers can offer efficient charge transfer through the S−M interface by means of electron tunneling and improve the charge collection (Figure 5). Since the photocurrent is generally low, charge transfer through the TiO_2−CNT by thermionic emission seems impossible.[30] As a result, the carbon conductors hardly have

DOI: 10.1021/jacs.5b13464
J. Am. Chem. Soc. 2016, 138, 3183−3189

any benefit to the charge transport or charge collection. The slight decrease in photocurrent for the CNT/TiO_2 electrode should be ascribed to the leakage of the photogenerated electrons via the naked carbon nanostructures (Figure 5).[56]

To further popularize the resultant energy savings of electron tunneling in PEC applications, we demonstrate the virtue of our electrode configuration in visible light driven water splitting. Similar to the situation of dye-sensitized photovoltaic devices, the cell with CNT|Nb-TiO_2(t) incorporated electrode exhibits the best performance for hydrogen evolution, showing the highest photocurrent over the measured range and a plateau current density of ~4.6 mA/cm^2 over the potential window of −1.0 to −0.3 V vs SCE (Figure 6). Following a descending order in performance is the cell incorporated with CNT|TiO_2(t), which exhibits a plateau current density of 3.7 mA/cm^2. The cell with plain TiO_2 electrodes exhibits the lowest plateau current density of 2.4 mA/cm^2. For the cell using CNT/TiO_2 electrodes, the plateau current density is 3.1 mA/cm^2. Compared with the case of a plain TiO_2 electrode (Figure 5), the higher photocurrent for the CNT/TiO_2 cells suggests that a certain percentage of photogenerated electrons can overcome the potential barrier following the thermionic emission at such current density, which is in good agreement with the relationship of D_n−J_{SC} for the dye-sensitized solar cells as shown in Figure 4c.

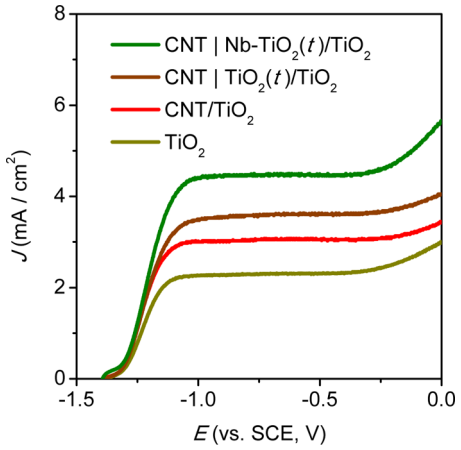

Figure 6. Voltammetric behaviors of the PEC cells based on CdS quantum dot-sensitized TiO_2 electrodes under AM 1.5G illumination.

3. CONCLUSION

In this work, we have studied the role of tunneling interlayers in the carbon conductors incorporated semiconductor electrodes as an effective way to save the energy from excessive internal dissipation, which many metal oxides encounter during transfer of charges over the potential barriers by thermionic emission. We have employed a CNT-TiO_2 contact as the model system to demonstrate the charge-transfer behaviors and related energy consumption. On the basis of theoretical simulation, we found that the electron tunneling could effectively save the energy dissipation for charge transfer through the metal−semiconductor interface and fully exert the role of the charge transport channels, which is in good agreement with the charge diffusion parameters. By application of tunneling interlayers into the CNTs incorporated TiO_2 electrodes, the facilitated S−M interfacial transfer of charges can improve charge transport and collection in every circumstance of high (photovoltaic devices), mediate (visible light induced water splitting), and low (UV induced water splitting) current densities. We believe that our work can also prompt the sequential development of perovskite solar cells, energy storage devices, oxygen evolution reactions, and other relevant applications, in which metal oxides are employed.

■ ASSOCIATED CONTENT

Supporting Information

The Supporting Information is available free of charge on the ACS Publications website at DOI: 10.1021/jacs.5b13464.

Simulation and Experimental details, Figures S1−S13 (PDF)

■ AUTHOR INFORMATION

Corresponding Authors

*zpzhu@sxicc.ac.cn

*liubin@ntu.edu.sg

Notes

The authors declare no competing financial interest.

■ ACKNOWLEDGMENTS

The authors acknowledge A*Star (M4070178.120), Nanyang Technological University (M4080977.120), State Key Laboratory of Coal Conversion (J15-16-913), and Ministry of Education of Singapore (M4011021.120) for the financial support. J.C. thanks Dr. Yinghua Xu (Zhejiang Univ. Technol.) and Dr. Tiancheng Xu (HzCell Electrochem. Corp.) for the help on discussion of photoelectrochemical results. Acknowledgements are also given to Dr. Kedar Hippalgaonkar and Dr. Chiam Sing Yang (Institute of Materials Research and Engineering, A*Star) for the XPS measurements.

■ REFERENCES

(1) Chen, C. T.; Cahan, B. D. *J. Electrochem. Soc.* **1982**, *129*, 17.
(2) Lyons, M. E. G.; Brandon, M. P. *J. Electroanal. Chem.* **2009**, *631*, 62.
(3) Jin, H.; Wang, J.; Su, D.; Wei, Z.; Pang, Z.; Wang, Y. *J. Am. Chem. Soc.* **2015**, *137*, 2688.
(4) Liang, H.; Meng, F.; Cabán-Acevedo, M.; Li, L.; Forticaux, A.; Xiu, L.; Wang, Z.; Jin, S. *Nano Lett.* **2015**, *15*, 1421.
(5) Morales-Guio, C. G.; Mayer, M. T.; Yella, A.; Tilley, S. D.; Grätzel, M.; Hu, X. *J. Am. Chem. Soc.* **2015**, *137*, 9927.
(6) Hagfeldt, A.; Boschloo, G.; Sun, L. C.; Kloo, L.; Pettersson, H. *Chem. Rev.* **2010**, *110*, 6595.
(7) Liu, B.; Aydil, E. S. *J. Am. Chem. Soc.* **2009**, *131*, 3985.
(8) Qian, F.; Wang, G.; Li, Y. *Nano Lett.* **2010**, *10*, 4686.
(9) Yang, X.; Wolcott, A.; Wang, G.; Sobo, A.; Fitzmorris, R. C.; Qian, F.; Zhang, J. Z.; Li, Y. *Nano Lett.* **2009**, *9*, 2331.
(10) Ling, Y.; Wang, G.; Wheeler, D. A.; Zhang, J. Z.; Li, Y. *Nano Lett.* **2011**, *11*, 2119.
(11) Wang, G.; Wang, H.; Ling, Y.; Tang, Y.; Yang, X.; Fitzmorris, R. C.; Wang, C.; Zhang, J. Z.; Li, Y. *Nano Lett.* **2011**, *11*, 3026.
(12) Wang, Q.; Zhang, Z.; Zakeeruddin, S. M.; Gratzel, M. *J. Phys. Chem. C* **2008**, *112*, 7084.
(13) Chandiran, A. K.; Sauvage, F.; Casas-Cabanas, M.; Comte, P.; Zakeeruddin, S. M.; Graetzel, M. *J. Phys. Chem. C* **2010**, *114*, 15849.
(14) Lu, X. J.; Mou, X. L.; Wu, J. J.; Zhang, D. W.; Zhang, L. L.; Huang, F. Q.; Xu, F. F.; Huang, S. M. *Adv. Funct. Mater.* **2010**, *20*, 509.
(15) Hu, Y.; Su, Y.; Huang, H.; Qian, Q.; Guan, Z.; Feng, J.; Li, Z.; Zou, Z. *ChemCatChem* **2015**, *7*, 2979.
(16) Sun, J.; Memon, M. A.; Bai, W.; Xiao, L.; Zhang, B.; Jin, Y.; Huang, Y.; Geng, J. *Adv. Funct. Mater.* **2015**, *25*, 4334.
(17) Tu, X.; Luo, S.; Chen, G.; Li, J. *Chem. - Eur. J.* **2012**, *18*, 14359.

DOI: 10.1021/jacs.5b13464
J. Am. Chem. Soc. 2016, 138, 3183−3189

(18) Kongkanand, A.; Martínez Domínguez, R.; Kamat, P. V. *Nano Lett.* **2007**, *7*, 676.
(19) Kamat, P. V. *J. Phys. Chem. Lett.* **2011**, *2*, 242.
(20) Chen, T.; Qiu, L.; Cai, Z.; Gong, F.; Yang, Z.; Wang, Z.; Peng, H. *Nano Lett.* **2012**, *12*, 2568.
(21) Tang, Y. B.; Lee, C. S.; Xu, J.; Liu, Z. T.; Chen, Z. H.; He, Z. B.; Cao, Y. L.; Yuan, G. D.; Song, H. S.; Chen, L. M.; Luo, L. B.; Cheng, H. M.; Zhang, W. J.; Bello, I.; Lee, S. T. *ACS Nano* **2010**, *4*, 3482.
(22) Yang, N. L.; Zhai, J.; Wang, D.; Chen, Y. S.; Jiang, L. *ACS Nano* **2010**, *4*, 887.
(23) Kamat, P. V.; Tvrdy, K.; Baker, D. R.; Radich, J. G. *Chem. Rev.* **2010**, *110*, 6664.
(24) Hayashi, H.; Lightcap, I. V.; Tsujimoto, M.; Takano, M.; Umeyama, T.; Kamat, P. V.; Imahori, H. *J. Am. Chem. Soc.* **2011**, *133*, 7684.
(25) Dang, X.; Yi, H.; Ham, M.-H.; Qi, J.; Yun, D. S.; Ladewski, R.; Strano, M. S.; Hammond, P. T.; Belcher, A. M. *Nat. Nanotechnol.* **2011**, *6*, 377.
(26) Chen, R.; Wang, H.-Y.; Miao, J.; Yang, H.; Liu, B. *Nano Energy* **2015**, *11*, 333.
(27) Zhu, K.; Neale, N. R.; Miedaner, A.; Frank, A. J. *Nano Lett.* **2007**, *7*, 69.
(28) Zhu, K.; Vinzant, T. B.; Neale, N. R.; Frank, A. J. *Nano Lett.* **2007**, *7*, 3739.
(29) Jennings, J. R.; Ghicov, A.; Peter, L. M.; Schmuki, P.; Walker, A. B. *J. Am. Chem. Soc.* **2008**, *130*, 13364.
(30) Chen, J.; Li, B.; Zheng, J.; Zhao, J.; Zhu, Z. *J. Phys. Chem. C* **2012**, *116*, 14848.
(31) Villanueva-Cab, J.; Jang, S.-R.; Halverson, A. F.; Zhu, K.; Frank, A. J. *Nano Lett.* **2014**, *14*, 2305.
(32) Chen, J.; Yang, H. B.; Miao, J.; Wang, H.-Y.; Liu, B. *J. Am. Chem. Soc.* **2014**, *136*, 15310.
(33) Roy-Mayhew, J. D.; Aksay, I. A. *Chem. Rev.* **2014**, *114*, 6323.
(34) Jariwala, D.; Sangwan, V. K.; Lauhon, L. J.; Marks, T. J.; Hersam, M. C. *Chem. Soc. Rev.* **2013**, *42*, 2824.
(35) Huang, X.; Qi, X. Y.; Boey, F.; Zhang, H. *Chem. Soc. Rev.* **2012**, *41*, 666.
(36) Costa, R. D.; Lodermeyer, F.; Casillas, R.; Guldi, D. M. *Energy Environ. Sci.* **2014**, *7*, 1281.
(37) Ng, Y. H.; Lightcap, I. V.; Goodwin, K.; Matsumura, M.; Kamat, P. V. *J. Phys. Chem. Lett.* **2010**, *1*, 2222.
(38) Brown, P.; Takechi, K.; Kamat, P. V. *J. Phys. Chem. C* **2008**, *112*, 4776.
(39) Ni, M.; Leung, M. K. H.; Leung, D. Y. C.; Sumathy, K. *Sol. Energy Mater. Sol. Cells* **2006**, *90*, 2000.
(40) Kron, G.; Egerter, T.; Werner, J. H.; Rau, U. *J. Phys. Chem. B* **2003**, *107*, 3556.
(41) Sze, S. M.; Ng, K. K. *Physics of Semiconductor Devices*; 3rd ed.; John Wiley & Sons: Hoboken, 2007.
(42) Viswanathan, V.; Pickrahn, K. L.; Luntz, A. C.; Bent, S. F.; Nørskov, J. K. *Nano Lett.* **2014**, *14*, 5853.
(43) Kim, J.; Kim, B.-K.; Cho, S. K.; Bard, A. J. *J. Am. Chem. Soc.* **2014**, *136*, 8173.
(44) Hill, C. M.; Kim, J.; Bard, A. J. *J. Am. Chem. Soc.* **2015**, *137*, 11321.
(45) Shiraishi, M.; Ata, M. *Carbon* **2001**, *39*, 1913.
(46) Guo, W.; Xu, C.; Wang, X.; Wang, S.; Pan, C.; Lin, C.; Wang, Z. L. *J. Am. Chem. Soc.* **2012**, *134*, 4437.
(47) Manga, K. K.; Zhou, Y.; Yan, Y. L.; Loh, K. P. *Adv. Funct. Mater.* **2009**, *19*, 3638.
(48) Kusumawati, Y.; Martoprawiro, M. A.; Pauporté, T. *J. Phys. Chem. C* **2014**, *118*, 9974.
(49) Brown, P.; Takechi, K.; Kamat, P. V. *J. Phys. Chem. C* **2008**, *112*, 4776.
(50) Xiang, Z. H.; Zhou, X.; Wan, G.; Zhang, G. X.; Cao, D. P. *ACS Sustainable Chem. Eng.* **2014**, *2*, 1234.
(51) Neamen, D. *An Introduction to Semiconductor Devices*; McGraw-Hill, Inc.: New York, 2006.
(52) Peter, L. M. *Chem. Rev.* **1990**, *90*, 753.
(53) Wang, H.-Y.; Chen, J.; Xiao, F.-X.; Zheng, J.; Liu, B. *J. Mater. Chem. A* **2016**, DOI: 10.1039/C5TA08202A.
(54) Livage, J.; Henry, M.; Sanchez, C. *Prog. Solid State Chem.* **1988**, *18*, 259.
(55) Swamy, V.; Kuznetsov, A.; Dubrovinsky, L. S.; Caruso, R. A.; Shchukin, D. G.; Muddle, B. C. *Phys. Rev. B: Condens. Matter Mater. Phys.* **2005**, *71*, 184302.
(56) Kyaw, A. K. K.; Tantang, H.; Wu, T.; Ke, L.; Peh, C.; Huang, Z. H.; Zeng, X. T.; Demir, H. V.; Zhang, Q.; Sun, X. W. *Appl. Phys. Lett.* **2011**, *99*, 021107.
(57) Ruhle, S.; Cahen, D. *J. Phys. Chem. B* **2004**, *108*, 17946.

DOI: 10.1021/jacs.5b13464
J. Am. Chem. Soc. 2016, 138, 3183−3189